water

MDPI

Article

Dynamics of Infiltration Rate and Field-Saturated Soil Hydraulic Conductivity in a Wastewater-Irrigated Cropland

Si-Yi Zhang [1,2], Isaac Hopkins [2], Li Guo [2] and Henry Lin [2,*]

[1] Guangdong Key Laboratory of Integrated Agro-environmental Pollution Control and Management, Guangdong Institute of Eco-environmental Science and Technology, Guangzhou 510650, China

[2] Department of Ecosystem Science and Management, The Pennsylvania State University, University Park, PA 16802, USA

* Correspondence: henrylin@psu.edu

Received: 12 June 2019; Accepted: 3 August 2019; Published: 7 August 2019

Abstract: The maintenance of a soil's infiltration rate (*IR*) and field-saturated hydraulic conductivity (K_{fs}) is crucial for the long-term sustainable functioning of wastewater-irrigated lands. However, an effective procedure for reliably measuring in situ soil K_{fs} remains elusive. To address this issue, this study investigated the dualhead infiltrometer (DHI), a novel instrument for automatically determining *IR* and K_{fs}, and compared it with a traditional double-ring infiltrometer (DRI) under various field conditions. In the initial phase, we optimized the procedure and settings for the DHIs in a cropland that was spray-irrigated with secondary-treated wastewater for decades in central Pennsylvania. Results showed that our optimized procedure, which used a single, long pressure cycle, yielded more robust measurements of *IR* than the originally recommended sequence of two short pressure cycles. The values of K_{fs} measured by the DHIs with optimized settings were similar to those measured by DRIs under many (but not all) field conditions, due to their differences in infiltration surface areas, operational procedures, length of infiltration time, and soil spatiotemporal variability. Viscosity-corrected K_{fs} on the irrigated cropland was 123.8 ± 94.0 mm·h^{-1}, higher than that on the adjacent non-irrigated cropland (103.2 ± 94.6 mm·h^{-1}), but the difference was not statistically significant, owing to the high degree of soil spatiotemporal variability and our limited number of measurements. Nevertheless, the higher K_{fs} values measured on irrigated cropland reflect observed changes in soil structure (e.g., soil pore characteristics) that resulted from decades of irrigation. Seasonal variations in K_{fs} values existed between winter and summer conditions, but *IR*s during all seasons remained much higher than the current spray-irrigation rate (4.25 mm·h^{-1}), suggesting that the soil is still capable of handling the routine irrigation, even during winter. However, the coefficients of variation exceeded 67.0% across the field sites investigated, and the time periods covered by our measurements were limited. As this specific site is permitted to discharge treated wastewater year-round, caution must still be exercised to ensure that soil K_{fs} remains high enough to prevent runoff generation, especially during winter frozen conditions.

Keywords: hydropedology; soil physics; soil moisture; soil temperature; wastewater irrigation; infiltrometer

1. Introduction

Many soil physical, chemical, and biological factors influence infiltration rate (*IR*) and field-saturated soil hydraulic conductivity (K_{fs}), both of which show significant variations across space and time [1,2]. Porosity and pore size distribution are among the major controlling factors of the rate of

water flow in soils [3]. For instance, greater macroporosity often gives rise to a higher *IR* [4]. High temperatures increase *IR*s by changing the viscosity and surface tension of the infiltrating water [3,5,6]. A higher antecedent soil moisture limits the *IR* [7,8]. Vegetation and land use can also alter soil characteristics, such as aggregation, organic matter content, compaction, and pore size distribution, all of which impact soil hydraulic conductivity [3,9]. For example, vegetation canopies and leaf litter can maintain the infiltration capacity of forest soils by protecting the soil surface from the impact of raindrops and preventing the formation of surface crusts, while roots induce the formation of macropores that improve the soil's macroporosity and infiltration capacity [10,11].

In addition to spatial variations due to site-specific conditions, soil *IR* and K_{fs} also experience temporal dynamics. For instance, hydraulic conductivity is often higher in the dry season than in the wet season [12,13], and higher in the summer than in the winter [14,15]. Soil infiltration at high latitudes or elevations is affected by frequent freeze–thaw cycles [16] and the presence of ice-rich layers, which can impede infiltration during winter [17].

Wastewater irrigation is a cost-effective and sustainable water resource management practice that is gaining attention as the world faces a looming freshwater crisis [18]. One priority of long-term wastewater irrigation operations is to maintain adequate soil infiltration capacity and K_{fs}, which may vary with soil type, water quality, and management practices [19,20]. While some researchers identified benefits of applying treated wastewater irrigation on soil properties, such as reductions in bulk density, greater aggregate stability, and increases in organic matter content [20,21], other studies found no such improvements or identified adverse effects, such as reduced infiltration capacity [22–25]. In terms of soil hydraulic properties, both positive and negative influences were reported. For example, Hati et al. [20] and Vogeler [21] reported increases in saturated and unsaturated hydraulic conductivity, respectively, after treated wastewater irrigation, while Wang et al. [25], Coppola et al. [26], and Gharaibeh et al. [27] found that infiltration rates, permeability, and saturated hydraulic conductivity declined with the application of treated wastewater effluent, respectively. An increase in total porosity, a larger mean weight diameter of aggregates, and a lower bulk density could increase hydraulic conductivity, whereas increased retention parameters and bulk density, or pore occlusion due to migrated clayey material could reduce hydraulic conductivity [20,21,27,28]. The balance of these effects will determine the net change in soil hydraulic conductivity, which is likely to be highly dependent on local conditions and management practices.

Since 1962, Penn State irrigated its secondary-treated wastewater on a specific area of cropped and forested land [29]. The naturally thick soils chosen for this purpose effectively acted as a "living filter" to provide tertiary—and final—treatment of the treated wastewater (Figure 1). During the period from 1962 through 1976, this land-based spray irrigation system was investigated as a small-scale test site. In 1983, it was expanded into a much larger and full-scale wastewater-treatment operation. As a result, Pennsylvania State University stopped discharging its effluent directly into the local watershed tributaries. Instead, the treated wastewater was spray-irrigated year-round to provide (1) tertiary effluent treatment before the treated wastewater enters into water bodies (water quality protection), (2) re-use of nutrients for crop production and tree growth (nutrient management), and (3) enhanced recharge to the groundwater to re-supply water to wells (water quantity conservation).

Traditional wastewater disposal generally focuses on direct discharge and on treatment methods designed to achieve levels of effluent quality that are acceptable for discharge. However, regulations aimed at reducing water resource degradation require that environmentally sound and cost-effective non-discharge alternatives must be considered and used. Environmental consciousness and emerging technologies for non-discharge wastewater management alternatives evolved over time. Recycling wastewater for re-use and returning treated wastewater to groundwater aquifers by land application emerged as strategies to respond to this need. Non-discharge practices constitute good environmental management, and states in the United States (US) are required to adopt an anti-degradation policy that meets minimum requirements. They must include this policy as a required element of their surface water quality standards programs in order to gain federal approval of the standards.

In general, subsurface wastewater treatment applications offer numerous advantages [30]. These systems typically require a low degree of maintenance and the energy requirements are also low. Temperature equilibration of water is achieved during subsurface storage and excursions in water quality are buffered due to dispersion in the subsurface and dilution with native groundwater. The "living filter" allows reclaimed water to infiltrate slowly through the vadose zone, where sorption, filtration, and biodegradation can enhance the water quality (also called soil aquifer treatment [30]). To maintain soil infiltrability during operation with reclaimed water, and for mosquito control, wastewater spray fields are usually operated in alternate wet and dry cycles. As spray fields dry out, dissolved oxygen penetrates into the subsurface, thereby facilitating biochemical transformation processes, and organic material accumulated on the soil surface will decompose, allowing for the recovery of infiltration rates [31].

Following years of research in Pennsylvania's northern climate, and experimentation with various application rates (2.54, 5.08, 10.16, and 15.24 cm/week), a 5.08-cm/week (i.e., two inches/week) rate was selected for year-round use in the "living filter" [32]. As a 5.08-cm/week spray rate is generally applied over a 12-h period, once per week (the rest of week, the soil is rested to dry out), which is equivalent to 4.25 mm of effluent per hour [33]. Each lateral at the "living filter" is only turned on for between 25 and 35 irrigations each year, resulting in an average annual effluent of about 1500 mm [33]. Two large spray fields were carefully chosen for this purpose. These sites are underlain by thick residual soils derived from weathered carbonate rock and a deep water table [32]. Irregular surface topography, resulting from the differential weathering of carbonate bedrock, ensures retention, infiltration, and recharge of effluent.

Many methods and infiltrometer designs were used to measure *IR* and to calculate K_{fs} [34,35]. To alleviate some of the difficulties encountered with reliable and automatic measurements, dualhead infiltrometers (DHIs) [36] were developed based on falling-head measurements [37]. These DHIs measure K_{fs} using two pressure heads, which are controlled by air pressure rather than the water ponding depth. To date, this automated device was subjected to limited field testing (e.g., Reference [38]). Previous studies typically applied the instrument using the default settings recommended by the manufacturer (e.g., References [39,40]). Therefore, its performance, optimal measurement procedures, and related parameterization under various field conditions need more field tests.

The objectives of this study were to (1) compare the performance of the new DHI using original and optimized settings; (2) compare the results from the DHI with those from classic double-ring infiltrometers (DRI); (3) investigate the seasonal dynamics of K_{fs}, especially under winter and summer conditions; and (4) determine if, and to what extent, the long-term irrigation of wastewater influenced K_{fs} and its spatiotemporal dynamics, and particularly the long-term sustainability of the living filter.

2. Materials and Methods

2.1. Study Sites

The study area is located in the Pennsylvania State University's "living filter" in central Pennsylvania (Figure 1), at an elevation of about 335 m. The climate is a composite of the relatively dry midwestern continental climate and the more humid conditions found near the eastern seaboard [41]. Mean monthly air temperature peaks in July (22.2 °C) and bottoms in January (−2.8 °C), with daily minimum air temperature generally remaining below freezing from November through March. Mean annual precipitation is 932.4 mm, with the most precipitation occurring in May (101.6 mm) and the least in January (59.4 mm). Annually, the study sites receive a total of about 2.5 m of water (irrigation plus natural precipitation), resulting in a "northern rainforest" [33]. The living filter is situated on a thick (up to 100 m) residual limestone-derived Hagerstown silt loam soil [42]. It is well drained with moderate permeability [29]. The regional water table is roughly 60 m below the land surface [43].

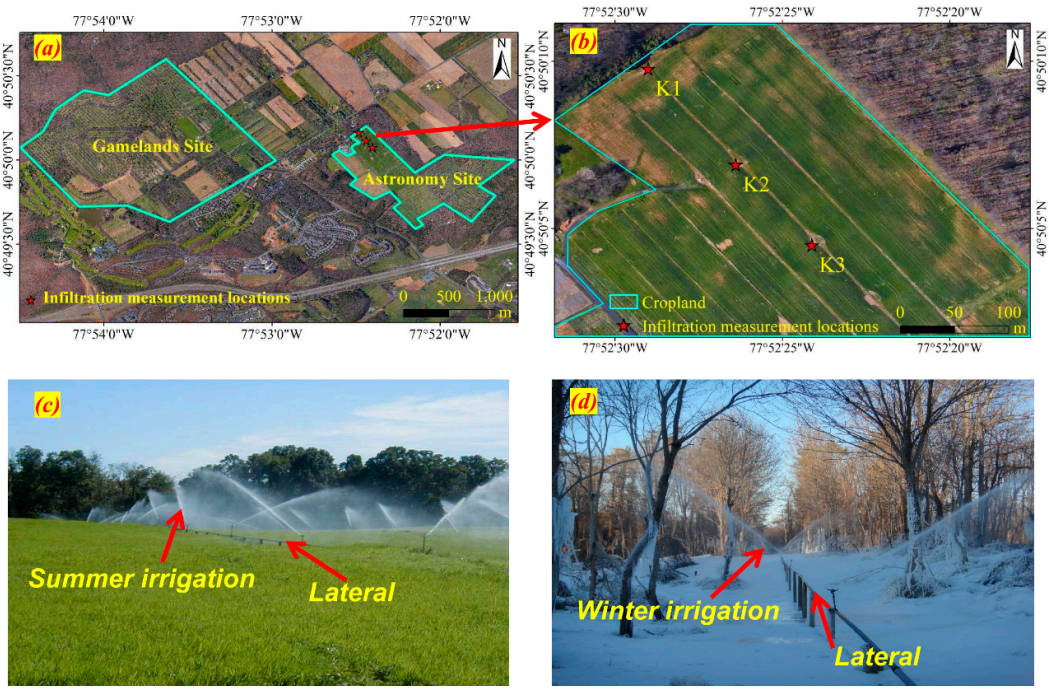

Figure 1. Penn State's "living filter," located in central Pennsylvania (**a**), with two fields—one is the State Game Land site (425 acres), and the other is the Astronomy site (182 acres); altogether, there are ~66% forested and ~34% cropped lands. The zoomed-in map (**b**) shows the cropped portion of the Astronomy site and indicates the infiltration measurement locations (K1, K2, and K3). Also included are photos demonstrating the operation of the living filter during the (**c**) summer and (**d**) winter.

Selected chemical properties of the treated wastewater are shown in Table 1 [44]. The no-till cropland is planted with an annual rotation of corn (*Zea mays* L.) and wheat (*Triticum aestivum* L.). Three sites were used to measure K_{fs} (Figure 1): a control site, K1, located on the northwest margin of the cropland but outside the range of the irrigation; and two experimental sites, K2 and K3, located within the irrigated cropland. The distance between neighboring sites was approximately 100 m.

Table 1. Average chemical characteristics of the municipal wastewater used for irrigation from November 2005 until August 2006 (n = 21) [44].

Parameter (Unit)	Values
Total alkalinity (mg·L^{-1} as $CaCO_3$)	179
Biological oxygen demand (mg·L^{-1})	8
Specific conductance (μmhos·cm^{-1})	1109
Total hardness (mg·L^{-1} as $CaCO_3$)	245
pH	7
Total suspended solids (mg·L^{-1})	5
Nitrate (mg·L^{-1} as N)	12

2.2. Field-Saturated Soil Hydraulic Conductivity Measurements by DHIs

2.2.1. Field Measurements

The K_{fs} was measured intermittently from February 2016 to June 2017 using DHIs (Figure 2a). The exact locations of infiltrations varied weekly to avoid repeated disturbance to the soil, but all infiltrations at each site were conducted within a 10-m^2 area on the flattest topography available. Leaves, large vegetative litter, and snow were carefully removed during the preparation of the soil surface for infiltration measurement. The 5-cm-deep, 7.5-cm-radius insertion ring (Figure 2a) was

gently hammered into the soil to ensure good contact with the soil and minimal disturbance. It was then checked to ensure that it was level in all orthogonal directions. Prior to data collection, ground surface conditions were recorded, and antecedent soil volumetric water content (VWC) and soil temperature (T_s) were measured nearby at a depth of 10 cm using ECH2O 5TE sensors (Meter Group, WA, USA). To measure the temperature of the infiltrating water (T_w) during the experiment, a thermometer was secured inside the chamber of the DHI before the infiltrometer head was clamped onto the insertion ring. Air temperature (T_a) was taken from the Rock Springs site of the Soil Climate Analysis Network (SCAN), 16 km away from the living filter [45].

The default measurement parameters and the device program were tested and then compared with optimized settings during the first few winter months of 2016. Subsequent infiltration experiments adopted only the optimized parameters (Table 2). The default procedure (for wet, loamy sand) included a 15-min soaking period and two cycles of 15-min holding times at the high and low pressure heads [36]. Our optimized procedure was implemented to better ensure that a steady state of infiltration was reached (a prerequisite for reliable K_{fs} measurements). It replaced the two short cycles with a single 35-min cycle at each pressure head (Table 2). The DHI recorded the water depth and pressure head (Figure 3), as well as the water flux per minute. During each infiltration experiment, the infiltrometer head was checked periodically to ensure that the seal was intact. If any sign of leakage or near-surface lateral flow occurred (for example, due to topography or frozen soil), the test was aborted. The ponding depth of the DHIs remained the same, at 5 cm, for both the lower and higher pressure heads, which was equal to the lower pressure head (5 cm). To achieve the higher pressure head (10 and 15 cm for the default and optimized setting, respectively), an air pump in the control unit (Figure 2a) was used to pump air into the sealed infiltrometer head (Figure 2a) to add air pressure.

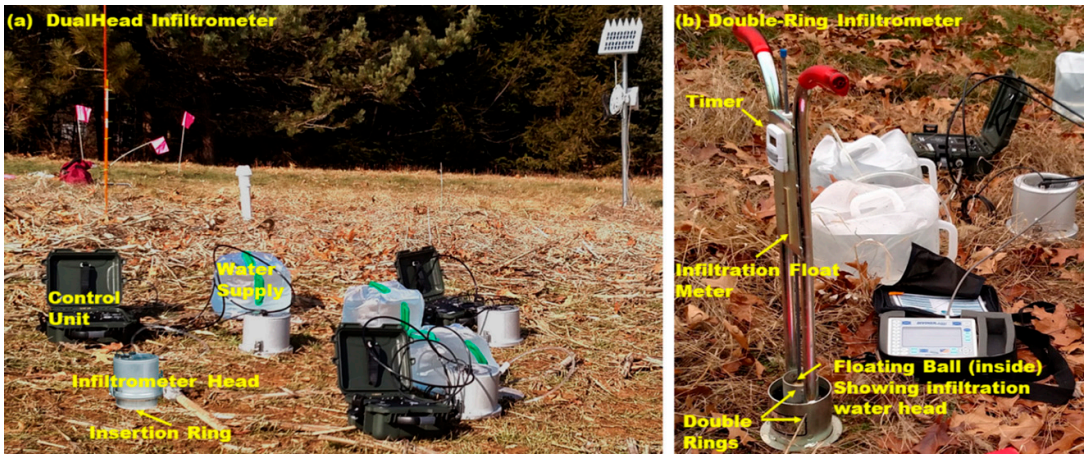

Figure 2. (**a**) Dualhead infiltrometers (DHIs) during a measurement (in triplicate) on the irrigated cropland, and (**b**) double-ring infiltrometer (DRI) during a measurement alongside a dualhead infiltrometer on the non-irrigated cropland.

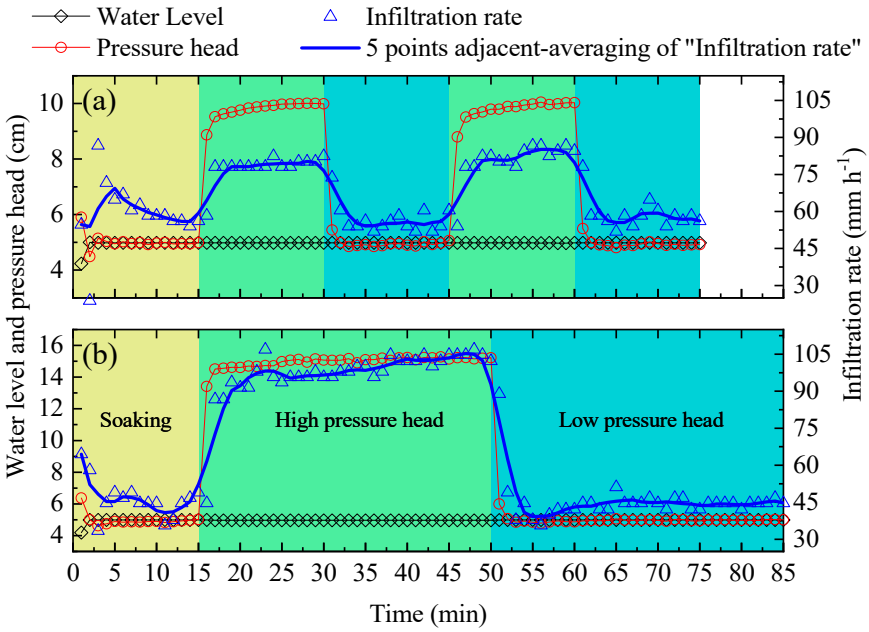

Figure 3. Examples of the raw data recorded during measurements using a DHI with (**a**) the default parameters and (**b**) the optimized parameters, as given in Table 2. The "5 points adjacent-averaging" line smoothed the data by averaging consecutive data points within a moving window of five points.

Table 2. Characteristics of eight infiltration processes with different measurement settings (default vs. optimized). CV_PH and CV_PL are the coefficients of variation (CV) for high and low pressure heads, respectively. CV_IH and CV_IL are the CVs for infiltration rates at high and low pressure heads, respectively. |Slp_H| and |Slp_L| are the absolute values of the linear regression slopes of the infiltration rate over time at high and low pressure heads, respectively. Different letters indicate a significant difference at $\alpha = 0.05$.

Parameters and Statistics		**Default (Original) Setting**	**Optimized (Modified) Setting**
Parameters	Soak time (min)	15	15
	Low pressure head (cm)	5	5
	High pressure head (cm)	10	15
	Hold time at each pressure head (min)	15	35
	Pressure cycles	2	1
	Total run time (min)	75	85
Statistics	CV_PH (%)	4.0 ± 3.2 [a]	0.9 ± 1.1 [b]
	CV_PL (%)	1.1 ± 0.4 [a]	1.2 ± 0.8 [a]
	CV_IH (%)	7.1 ± 4.5 [a]	3.0 ± 1.5 [b]
	CV_IL (%)	6.0 ± 3.9 [a]	4.5 ± 3.8 [a]
	|Slp_H| (mm·h^{-2})	75.5 ± 42.3 [a]	50.9 ± 61.9 [a]
	|Slp_L| (mm·h^{-2})	29.2 ± 33.7 [a]	17.6 ± 18.4 [a]
Number of test datasets used (see Figure 4)		8	8

2.2.2. Quality Controls

All data collected by the DHI were screened carefully to ensure quality. The coefficients of variation (CVs) of the pressure head and water level were calculated. As is common in statistical analysis, if a CV was greater than 15%, the data were considered unreliable and were subject to elimination [46]. In our case, this threshold was used to identify untrustworthy tests and measurements during which the pressure head, water level, or *IR* was not stable, possibly due to a poor seal. Considering that the *IRs* were recorded once per min, and this high frequency could record some high-frequency fluctuation of the *IRs*, some *IRs* may fluctuate within a range and did not show

a clear increasing or decreasing trend and, if they were resampled in 2 to 4 min, the CV of *IRs* could decrease greatly. Thus, if a measurement had a CV of raw *IRs* larger than 15% but lower than 50%, and the CV of resampled *IRs* was lower than 15%, then it was also thought to be reliable. Only the reliable measurements were used in further analysis.

2.2.3. Calculation of K_{fs}

The K_{fs} of soil was computed as follows [37]:

$$K_{fs} = \frac{i}{F}, \tag{1}$$

where i is the steady-state *IR* (mm·h^{-1}), and F is a function that corrects for soil sorptivity and the geometric effects of the infiltrometer. The function F was calculated using the method of Reynolds and Elrick [47] as follows:

$$F = 1 + \frac{\lambda + D}{C_1 d + C_2 b} = 1 + \frac{\lambda + D}{\Delta}, \tag{2}$$

where D is the ponding depth (mm), d is the insertion depth of the infiltrometer (cm), b is the infiltrometer radius (mm), Δ is a shape factor which is equal to $C_1 d + C_2 b$ (mm), C_1 is 0.993, C_2 is 0.578, and λ is the macroscopic capillary length of the soil (mm). Since K_{fs} was identical for both ponding depths (pressure heads), it was defined as

$$K_{fs} = \frac{i_1 \Delta}{\Delta + \lambda + D_1} = \frac{i_2 \Delta}{\Delta + \lambda + D_2}, \tag{3}$$

and the value of K_{fs} can be solved as

$$K_{fs} = \frac{\Delta(i_1 - i_2)}{D_1 - D_2}, \tag{4}$$

where Δ is a constant for a given infiltrometer geometry. For the DHI, d = 50 mm and b = 75 mm; thus, Δ = 93 mm. As recommended by Decagon Devices [36], only the data from the last cycle were used in the K_{fs} calculation, and the first two minutes of raw data after the pressure head changed were not used for calculating K_{fs}. To ensure comparability, a similar subset of pressure and infiltration records at each pressure head was used to calculate K_{fs} for the optimized measurements, even though the cycles took longer.

2.2.4. Viscosity Correction of K_{fs}

All K_{fs} values were viscosity-corrected to a standard temperature of 25 °C before comparing among different sites and different times to avoid the influence of changes in water effluent viscosity at different temperatures. K_{fs} may be split into two factors [48] as follows:

$$K_{fs} = k \times f, \tag{5}$$

where k is the intrinsic permeability of soil (m^2), and f is the fluidity of water (m^{-1}·s^{-1}). The f parameter is inversely proportional to viscosity, as

$$f = \frac{\rho_w g}{\eta} = \frac{g}{\eta'}, \tag{6}$$

where ρ_w is the density of the water (kg·m^{-3}), g is gravitational acceleration (m·s^{-2}), η is the dynamic water viscosity (Pa·s), and η' is the water's kinematic viscosity (m^2·s^{-1}). The corrected K_{fs} was calculated as

$$K_{fs\_STD} = K_{fs\_OB} \frac{\eta'_{OB}}{\eta'_{STD}}, \tag{7}$$

where K_{fs_OB} is an observed K_{fs} value, and K_{fs_STP} is the K_{fs} value corrected to the standard temperature. η'_{OB} and η'_{STD} are the kinematic viscosity at the temperature when K_{fs_OB} was measured and at the standard temperature (25 °C), respectively, and each can be calculated as follows [49]:

$$\eta'_T = 1.98404 \times 10^{-6} \times e^{\frac{1825.85}{273+T}}, \quad (8)$$

where η'_T is the kinematic viscosity ($m^2 \cdot s^{-1}$) at temperature T (°C).

2.3. Measurement of K_{fs} by DRIs

The DRIs used for this study had an inner ring radius of 3.02 cm and an outer ring radius of 5.40 cm (Figure 2b). Each infiltration measurement was conducted for 85 min to match the total duration of the DHI procedure. The device was carefully pushed into the surface soil to minimize disturbance. After a soaking period, the water was manually poured into the device and the change in the water level was recorded every minute. The value of K_{fs} was calculated according to Philip's infiltration equation [50],

$$i(t) = St^{0.5} + At, \quad (9)$$

where $i(t)$ is the cumulative infiltration at time t, S is the sorptivity of the soil, and A is a hydraulic conductivity parameter. Previous studies [51,52] suggested that the value of A is between 2/3 K_{fs} and 1/3 K_{fs}, but usually closer to 1/3 K_{fs}. For this study, the K_{fs} measured by the DRI (K_{fs_DR}) was calculated as $K_{fs\_DR} = 3A$.

2.4. Statistical Analysis

The mean *IR*s and K_{fs} values of a period or a site were calculated along with their standard deviations and presented as means ± standard deviation. Independent sample *t*-tests with α set to 0.05 were used to compare the T_a, T_s, *VWC*, *IR*, and K_{fs} values measured at different sites and times, as well as the CVs of pressure heads and infiltration rates, and the absolute linear regression slopes of the infiltration rate over time. To satisfy the assumption of normality, log-transformed corresponding data were used in the *t*-tests. This analysis was completed using SPSS 17.0 (SPSS Inc., Chicago, IL, USA). Linear regressions between K_{fs} measured by DHIs and DRIs, between K_{fs} and T_w, and between VWC and K_{fs_STP} were fitted using OriginPro 2019b (OriginLab Corporation, Northampton, MA, USA.).

3. Results and Discussion

3.1. The Influence of DHI Holding Time

The default (original) and modified (optimized) DHI measurement parameters resulted in different infiltration patterns (Figure 3). Pressure head was not steady during the short high-head cycles, even during the second cycle (Figure 3a), and the CV of the high-pressure head was significantly higher for the default procedure than for the optimized procedure (Figure 3b, Table 2). Since higher pressures led to higher *IR*s, the performance improvement of the optimized procedure was more pronounced during the high-head cycles (Table 2). In addition, since the high pressure head was achieved by increasing air pressure rather than by pooling additional water [36], the quality of these tests depended on complete airtightness of the infiltrometer head. By contrast, the pressures and *IR*s during the low-pressure periods were not significantly different between the default and optimized programs (Table 2). This pressure was set equal to the nominal ponding depth; thus, it was achieved with actual water-level head, rather than extra air pressure. The duration of the default procedure afforded 15 measurements of *IR*, but the first two measurements at each pressure head were not used in the K_{fs} calculations, as recommended by the device manual. However, the third and fourth records were also often unsteady as they continued to be affected by the transition between heads (Figure 4). Moreover, *IR* could be expected to fluctuate in response to changes in the physical

conditions of the soil, such as the melting of ice, the release of trapped air bubbles, or the breakthrough of water into connected macropores. These processes could distort the data for several minutes at a time, making the true steady-state *IR* difficult to determine with such a short available time window. Anomalous time-steps were excluded from K_{fs} calculations, which sometimes left fewer than 10 records from which to calculate K_{fs}.

Figure 5 contains time-series plots of all successful infiltrations collected with the optimized procedure. These results are grouped by season and antecedent VWC conditions. Winter data were collected from November through March, and summer data were gathered in June and July. The soil was considered wet when its antecedent VWC was higher than 0.25 $m^3 \cdot m^{-3}$, while values below this cut-off were considered dry. Several anomalous data points are visible in these plots (e.g., measurement #22 at 39 min and measurement #33 at 73 min; Figure 5c,d).

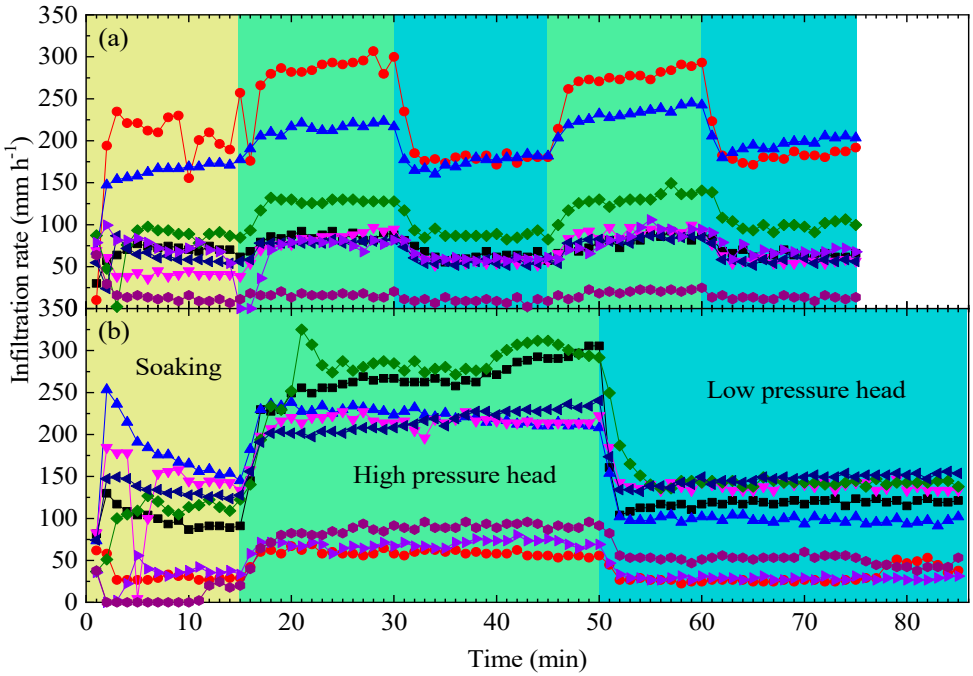

Figure 4. Infiltration rates of experiments conducted in winter months with (**a**) the default settings and (**b**) the optimized measurement parameters, as given in Table 2.

The optimized procedure, with its single long cycle, yielded better infiltration results than the default procedure for the silt loam in the living filter (Figure 2b). A long cycle increased the likelihood that the test reached a steady pressure head and *IR*, and it provided more of a buffer against fluctuations caused by transient changes in soil conditions (Figure 2b). Field applications of DHIs in soils heavier than a sandy loam may benefit from this improved approach: a 15-min soak time followed by 35 min held at a high pressure head, and then 35 min held at a low pressure head (Figure 3b). The *IR*s measured during the final 15 to 20 min of the hold time at each pressure head were generally usable for the calculation of K_{fs}.

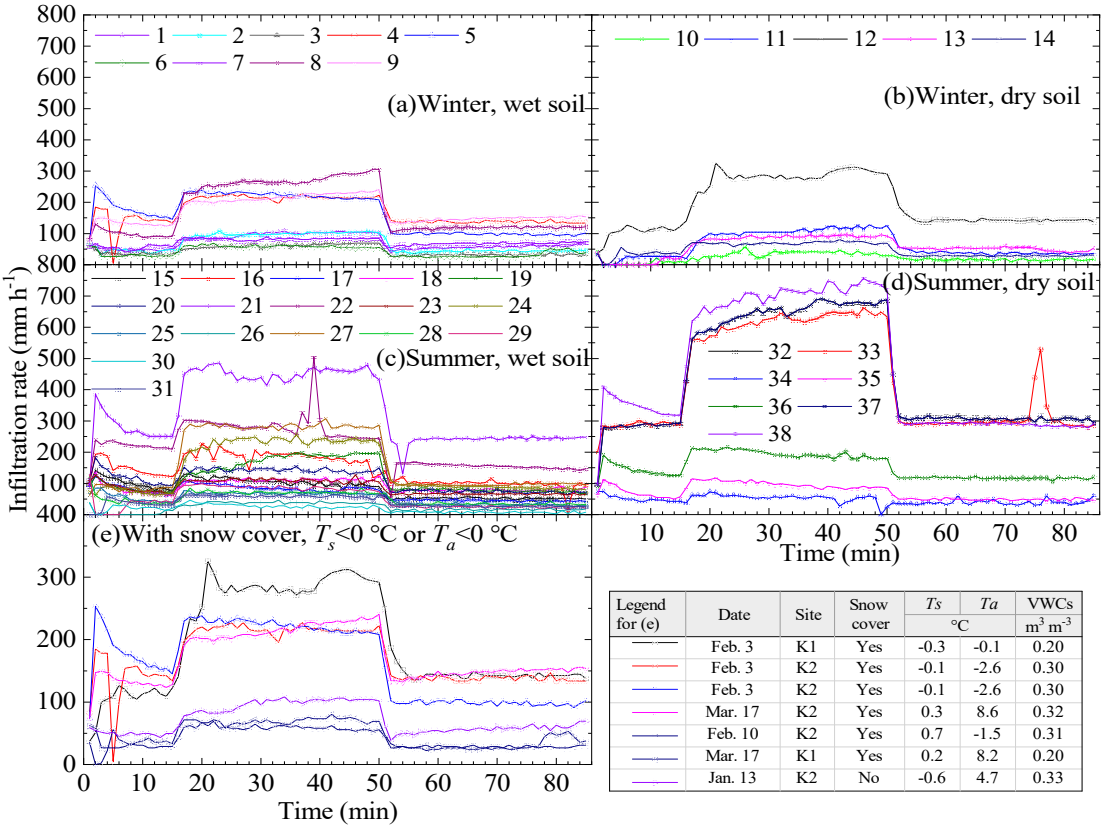

Legend for (e)	Date	Site	Snow cover	*Ts* °C	*Ta* °C	VWCs m^3 m^{-3}
	Feb. 3	K1	Yes	-0.3	-0.1	0.20
	Feb. 3	K2	Yes	-0.1	-2.6	0.30
	Feb. 3	K2	Yes	-0.1	-2.6	0.30
	Mar. 17	K2	Yes	0.3	8.6	0.32
	Feb. 10	K2	Yes	0.7	-1.5	0.31
	Mar. 17	K1	Yes	0.2	8.2	0.20
	Jan. 13	K2	No	-0.6	4.7	0.33

Figure 5. Infiltration rates under (**a**) wet and (**b**) dry soil moisture conditions and in winter (November to March), and under (**c**) wet and (**d**) dry soil moisture conditions in summer (June and July), and under (**e**) special conditions in winter (with snow cover, T_s < 0 °C, or T_a < 0 °C). Wet soil refers to an antecedent soil volumetric water content (VWC) higher than 0.25 m^3·m^{-3}, while dry soil had a VWC below this value. T_a is air temperature, and T_s is soil temperature. Each line represents a single infiltration run, with the legend numbered values corresponding to the "Number" column in Table 3.

3.2. Comparison of K_{fs} Measured by DHIs and DRIs

The values of K_{fs} measured by DHIs (K_{fs_DH}) and DRIs (K_{fs_DR}) on the same day are compared in Figure 6. Nine of 14 K_{fs} results were similar between the two methods (distributed along the 1:1 line). However, the other five K_{fs_DH} values were much higher than K_{fs_DR}. The regression line of all measurements has a slope of 1.15 mm·h^{-1} and an intercept of 13.45 mm·h^{-1}, showing that, on the whole, the DHI measured higher K_{fs} values than the DRI.

This difference between the performances of the two instruments may be explained by the larger footprint of the DHI. Kumar [3] also found that measured *IR* values were lower when using smaller DRIs. Lai and Ren [53] observed that smaller inner rings resulted in greater variability in K_{fs} measurements. The infiltration area of the DHI is 13.8 times that of the inner ring area of the DRI used in this study. This makes it less sensitive to the spatial heterogeneity of the soil and probably closer to the representative elementary volume of the experimental site, which reduces the effects of the measurement scale [53,54].

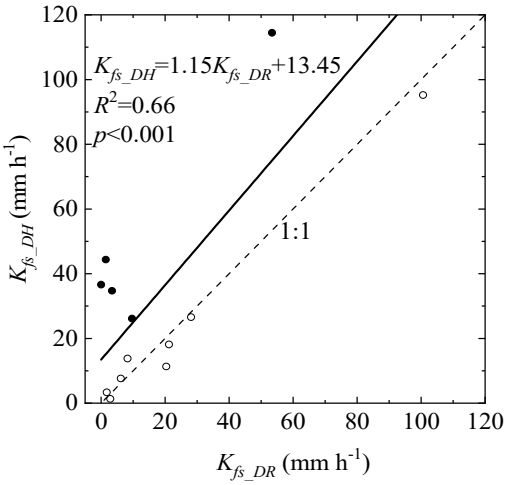

Figure 6. Relationship between field-saturated hydraulic conductivities measured concurrently by the DHI (K_{fs_DH}) and DRI (K_{fs_DR}). The solid dots indicate divergent measurements between the two methods, while the open dots, distributed along the 1:1 line (dashed), indicate similar results. All data were included in the regression line (solid). The equation, coefficient of determination (R^2), and the significance value (p) are also shown for the all-data regression (solid line).

On the other hand, smaller rings require a smaller area of flat topography and are more easily operated in sloped areas. The DHI uses a peristaltic pump in the control unit and a water-level sensor in the infiltrometer head (Figure 2a) to maintain the water level and measure the water flux. This is operator-friendly, but it also relies on an air pump to control the pressure head, which adds to the complexity and uncertainty of taking measurements of K_{fs}. During the collection of this dataset, about 40% of all measurement attempts failed, usually as a result of a compromised seal between the ring and the infiltrometer head, or a CV of the *IR* higher than 30%, leading to the inconsistent numbers of repetitions listed in Table 3.

Table 3. Date, site, air temperature (T_a), soil temperature (T_s), antecedent soil volumetric water content (VWC), infiltration rates at the higher and lower pressure head (*IR_H* and *IR_L*, respectively), and field-saturated soil hydraulic conductivity (K_{fs}) of measurements using the optimized parameters defined in Table 2. Corresponding raw infiltration data are graphically presented in Figure 5, and different backgrounds from top to bottom in this table correspond to Figure 5a, b, c, and d, respectively.

Number	Measurement Date	Site #	Effective Repetition	T_a °C	T_s °C	*VWC* $m^3 \cdot m^{-3}$	*IR_H* $mm \cdot h^{-1}$	*IR_LL* $mm \cdot h^{-1}$	K_{fs} $mm \cdot h^{-1}$
1	13 January 2017	K2	1	4.7	−0.6	0.33	103.7	61.3	41.8
2	27 January 2017	K2	1	1.6	1.5	0.32	67.3	32.2	32.4
3	27 January 2017	K2	2	1.6	1.5	0.32	103.6	44.4	51.1
4	3 February 2017	K2	1	−2.6	0.0	0.30	213.4	96.7	117.4
5	3 February 2017	K2	2	−2.6	0.0	0.30	215.3	137.0	73.1
6	10 February 2017	K2	1	−1.5	0.7	0.31	56.7	38.4	26.1
7	26 February 2017	K2	1	0.9	3.0	0.33	83.6	70.0	13.8
8	26 February 2017	K2	2	0.9	3.0	0.33	287.2	120.3	140.4
9	17 March 2017	K2	1	8.6	0.3	0.32	230.2	152.1	64.8
10	13 January 2017	K1	1	3.7	0.6	0.21	19.1	37.3	16.1
11	13 January 2017	K1	2	3.7	0.6	0.21	64.8	119.2	35.6
12	3 February 2017	K1	1	−0.1	−0.3	0.20	133.2	298.3	142.3
13	3 March 2017	K1	2	3.4	3.9	0.22	34.7	91.6	46.5
14	17 March 2017	K1	1	8.2	0.2	0.20	38.5	72.6	28.4
15	7 June 2017	K2	1	14.7	17.3	0.27	49.3	94.8	50.8
16	7 June 2017	K2	2	14.7	17.3	0.27	78.8	168.8	90.8
17	7 June 2017	K2	3	14.1	17.3	0.27	38.5	80.6	42.7
18	26 June 2017	K2	1	18.8	19.1	0.31	30.2	113.0	79.9
19	26 June 2017	K2	2	20.4	20.8	0.31	90.0	191.9	73.8
20	29 June 2017	K2	1	22.6	20.4	0.30	65.5	139.2	70.5
21	29 June 2017	K2	2	19.8	18.7	0.30	193.0	460.8	245.2
22	7 June 2017	K3	1	15.1	17.2	0.27	116.6	274.5	148.4
23	29 June 2017	K3	1	24.4	22.5	0.30	40.0	107.5	65.4
24	7 June 2017	K1	1	14.3	17.2	0.33	137.5	235.9	83.4
25	12 June 2017	K1	1	26.7	24.8	0.26	33.2	66.5	31.6
26	21 June 2017	K1	1	20.8	19.8	0.31	20.4	37.2	16.3
27	21 June 2017	K1	2	20.8	19.8	0.31	173.5	284.4	98.8
28	26 June 2017	K1	1	17.6	18.3	0.31	35.4	70.9	32.9
29	26 June 2017	K1	2	18.8	19.1	0.31	58.0	80.8	23.5
30	29 June 2017	K1	1	19.8	18.7	0.29	18.8	24.0	7.1
31	29 June 2017	K1	2	19.1	18.3	0.29	29.7	57.5	26.5
32	3 June 2016	K2	1	7.1	22.9	0.18	311.4	680.1	304.9
33	3 June 2016	K2	2	6.0	22.2	0.18	284.0	643.0	325.0
34	12 June 2017	K2	1	26.7	26.2	0.18	13.2	45.0	40.6
35	12 June 2017	K2	2	26.7	26.2	0.18	45.4	86.6	48.7
36	12 June 2017	K3	1	26.7	26.0	0.18	72.0	184.3	116.1
37	3 June 2016	K1	1	7.1	22.9	0.23	284.0	643.0	325.0
38	3 June 2016	K1	2	4.6	20.5	0.23	367.2	730.5	284.4

3.3. Seasonal Dynamics of IRs and K_{fs}, and Their Influencing Factors

Under most conditions, *IRs* decreased over time during the 15-min soaking period (Figures 5a,c,d), with the notable exception of dry, winter conditions, when most measurements indicated a gradually increasing *IR* (Figure 5b). The increasing *IR* during the soaking step in cold, dry soil could be explained by an initial period of hydrophobicity caused by low temperatures and dry soil aggregates [55,56]. This effect would become less prominent as soil moisture rises during the soaking period. Under high pressure heads, the behavior of the *IR* depended on antecedent soil wetness: when the soil was wet, infiltration was likely to decline over time; when the soil was dry, *IR* tended to increase.

During winter, when the soil was wet, the *IR* values clustered into two groups (Figure 5a). One group had higher *IR*s of 236.5 ± 34.6 and 126.5 ± 23.7 $mm \cdot h^{-1}$ at the high and the low pressure heads, respectively. The other group had lower *IR*s of 83.0 ± 21.1 and 49.2 ± 15.4 $mm \cdot h^{-1}$ at the high and the low pressure heads, respectively. These pronounced differences may have been caused by spatial

heterogeneity of soil properties (e.g., macroporosity), as the exact location of the experiment changed weekly. Also, it could be attributable to unidentified systematic errors. As reported by Gamie and De Smedt [57] and many others, great variation in hydraulic conductivity, spanning four orders of magnitude, was observed within an area of 120 m × 120 m. They attributed this to the combination of sampling and measurement errors, randomness, preferential flow, and soil heterogeneity.

When the soil was dry and cold, we measured *IR*s that varied from 37.3 to 298.3 mm·h^{-1} at the high pressure head and from 16.1 to 142.3 mm·h^{-1} at the low pressure head (Figure 5b). During summer, when the soil was wet, the *IR*s at high and low pressure heads were 160.3 ± 119.4 and 74.7 ± 61.3 mm·h^{-1}, respectively (Figure 5c). When the soil was dry during summer, the *IR*s at high and low pressure heads were 423.0 ± 286.2 and 207.1 ± 122.1 mm·h^{-1}, respectively (Figure 5d). Three of the measurements under dry summer conditions were much higher than the other measurements.

During special winter conditions, such as periods with snow cover, air temperature (T_a) slightly lower than 0 °C (−2.6 °C < T_a < 0 °C), and soil temperature (T_s) slightly lower than 0 °C (−0.6 °C < T_s < 0 °C), *IR* values were 181.1 ± 95.5, 193.3 ± 87.6, and 207.7 ± 79.8 mm·h^{-1} at the high pressure head and 99.2 ± 54.4, 96.7 ± 44.3, and 109.4 ± 37.9 mm·h^{-1} at the low pressure head, respectively (Figure 5e). These *IR*s were not significantly different from results obtained on other experimental days during winter (Table 4). A measurement on 3 February 2017 detected the highest *IR* during winter, despite the presence of snow cover, as well as cold and dry conditions (T_a = −0.05 °C, T_s = −0.3 °C, and VWC = 0.20 m^3·m^{-3}; Figure 5b,c). These results indicate that low air temperature, slightly frozen soil, and the presence of snow cover do not seem to impede infiltration at the study site.

Table 4. Characteristics of infiltration processes under different conditions. T_a is air temperature, T_s is soil temperature, and VWC is initial soil volumetric water content. *IR*_H and *IR*_L are the infiltration rates measured at high and low pressure heads, respectively; K_{fs_OB} and K_{fs_STP} are the initial observed and viscosity-corrected field-saturated hydraulic conductivities, respectively. Different letters in the same column indicate significance groupings at $\alpha = 0.05$.

Conditions	Number of Times	T_a	T_s	*VWC*	*IR_H*	*IR_L*	K_{fs_OB}	K_{fs_STP}
		°C	°C	$m^3 \cdot m^{-3}$	$mm \cdot h^{-1}$	$mm \cdot h^{-1}$	$mm \cdot h^{-1}$	$mm \cdot h^{-1}$
Winter, dry soil	6	4.7 ± 4.9 ^{a}	1.5 ± 1.9 ^{ad}	0.21 ± 0.02 ^{a}	133.6 ± 94.3 ^{a}	56.4 ± 45.8 ^{a}	70.7 ± 46.3 ^{a}	88.3 ± 60.3 ^{a}
Winter, wet soil	9	2.7 ± 3.3 ^{a}	2.1 ± 1.3 ^{a}	0.31 ± 0.01 ^{b}	151.2 ± 85 ^{a}	83.6 ± 44.7 ^{a}	62.2 ± 45.0 ^{a}	88.0 ± 57.6 ^{a}
Summer, dry soil	7	17.1 ± 10.5 ^{b}	23.8 ± 2.3 ^{b}	0.19 ± 0.03 ^{a}	423.0 ± 286.2 ^{b}	207.1 ± 122.1 ^{b}	184.8 ± 141.0 ^{b}	206.8 ± 147.7 ^{b}
Summer, wet soil	17	18.9 ± 2.7 ^{b}	19.2 ± 1.5 ^{c}	0.30 ± 0.01 ^{b}	160.3 ± 119.4 ^{a}	74.7 ± 61.3 ^{a}	77.5 ± 57.4 ^{a}	90.1 ± 63.9 ^{a}
With snow	6	1.7 ± 5.3 ^{a}	0.2 ± 0.4 ^{d}	0.27 ± 0.06^{c}	181.1 ± 95.5 ^{ab}	99.2 ± 54.4 ^{ab}	75.1 ± 45.2 ^{a}	111.8 ± 62.8 ^{a}
$T_a < 0$ °C	4	−1.7 ± 1.2 ^{a}	0.1 ± 0.4 ^{a}	0.28 ± 0.05 ^{b}	193.3 ± 87.6 ^{ab}	96.7 ± 44.3 ^{ab}	88.5 ± 47.3 ^{a}	123.3 ± 63.3 ^{ab}
$T_s < 0$ °C	4	−0.1 ± 3.4 ^{a}	−0.2 ± 0.3 ^{d}	0.28 ± 0.06 ^{b}	207.7 ± 79.8 ^{ab}	109.4 ± 37.9 ^{ab}	88.5 ± 47.4 ^{a}	135.6 ± 60.9 ^{ab}

During winter, the mean K_{fs_OB} was 70.7 ± 46.3 mm·h^{-1} when the soil was dry and 62.2 ± 45.0 mm·h^{-1} when it was wet. The corresponding summer values were 184.8 ± 141.0 mm·h^{-1} and 77.5 ± 57.4 mm·h^{-1}, respectively (Table 4). After the viscosity correction, the mean winter K_{fs_STP} values were 88.3 ± 60.3 and 88.0 ± 57.0 mm·h^{-1} when the soil was wet and dry, respectively, while the corresponding summer values were 206.8 ± 147.7 and 90.1 ± 63.9 mm·h^{-1}, respectively (Table 4). In winter with snow cover, $T_a < 0$ °C, and $T_s < 0$ °C, the mean K_{fs_OB} values were 75.1 ± 45.2, 88.5 ± 47.3, and 88.5 ± 47.4 mm·h^{-1}, respectively, and the corresponding values of K_{fs_STP} were 111.8 ± 62.8, 123.3 ± 63.3, and 135.6 ± 60.9 mm·h^{-1}, respectively (Table 4). Independent sample *t*-tests showed that the K_{fs_OB} and K_{fs_STP} values during dry summer conditions were significantly higher than the others (Table 4).

The living filter is permitted by the Pennsylvania Department of Environmental Protection (PADEP) to operate year-round, rather than using storage during the non-growing season [33]. However, frozen soils are an important management concern in the living filter, as irrigation onto frozen soils could lead to ponding and surface runoff; the latter conditions could potentially lead to nutrient-rich water entering nearby surface waterbodies. To address this management concern, we collected real-time monitoring data since 2008, which indicated that frozen soil conditions do not seem to noticeably impede deep infiltration or significantly alter vertical flow. This implies that irrigation during frozen soil conditions may not adversely affect effluent treatment [58,59]. This is probably attributable to warmer temperatures associated with the effluent when the effluent was sprayed on frozen soils intensively and continuously, leading to locally permeable frozen surfaces. The depth and temporal extent of frozen conditions, as well as the infiltration status and subsurface water fluxes under frozen conditions, however, require further investigation.

There were significant linear relationships between the observed K_{fs} and T_w at both the irrigated and non-irrigated sites (e.g., K2 and K1, respectively; Figure 7). However, the viscosity-corrected K_{fs} showed no significant relationship with T_w, suggesting that the temperature correction was effective. Additionally, no significant relationships were found between K_{fs_OB}, K_{fs_STP}, and soil temperature at K1 or K2.

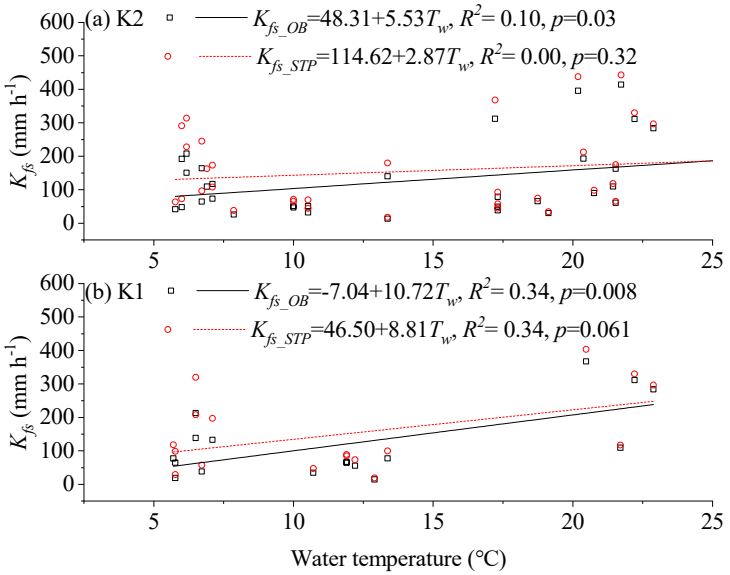

Figure 7. The relationship between K_{fs} and infiltrating water temperature at (**a**) K2 and (**b**) K1 sites. K_{fs}: field-saturated hydraulic conductivity; K_{fs_OB}: observed K_{fs}; K_{fs_STP}: K_{fs} that was viscosity-corrected to the standard temperature of 25 °C; T_w: water temperature.

The observed relationship between K_{fs} and T_w is consistent with previous studies [6,15,60,61], but the relationship between K_{fs} and soil temperature is different from the findings of Clancy and Alba [48], who found a significant linear relationship between the two variables. They suggested that soil

temperature could affect air viscosity and permeability, as the pore spaces of the field saturated soil are still between 5% and 20% occupied by air [62,63]. Air permeability is related to air viscosity and, thus, hydraulic conductivity correlates with soil temperature. However, we did not observe this association at the study site. Levy et al. [61] demonstrated that the effects of temperature on hydraulic conductivity were influenced by soil types. The results of this study suggest that the differences in K_{fs} at different temperatures were mainly controlled by the kinematic viscosity of water.

We observed a significantly negative linear relationship between K_{fs_STP} and antecedent VWC during winter, and across the whole experimental period, while such linear relationships were insignificant during summer (Figure 8). Similar linear relationships between K_{fs} and antecedent VWC were found in many studies. Because wet soils have reduced soil sorptivity, subsoil drainage is often restricted [13,64]. In addition, high soil VWC tends to cause clay-rich soils to swell, constricting soil cracks, decreasing soil macroporosity, and reducing macropore flow [4,13].

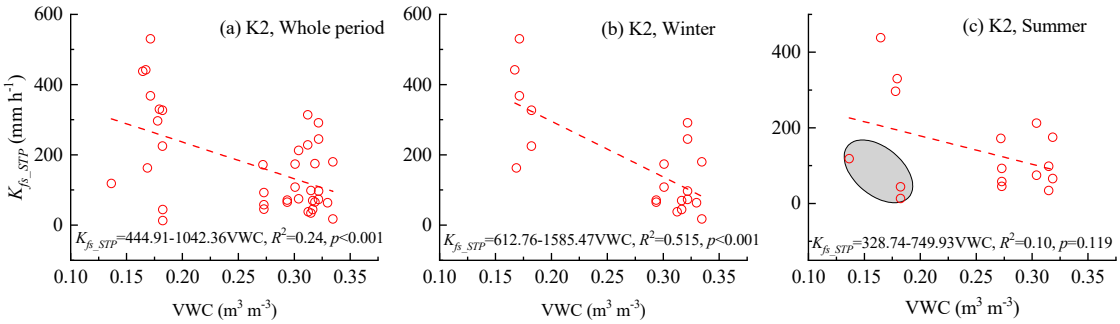

Figure 8. Relationships between antecedent soil volumetric water content (VWC) and viscosity-corrected field-saturated hydraulic conductivity (K_{fs_STP}) at K2 during the entire study duration (**a**), in the winter (**b**), and in the summer (**c**). The shaded region in (**c**) encompasses notably low K_{fs} values with the low soil VWC in the summer (included in the regression).

Two K_{fs} measurements on 12 June 2017 were extremely low. The surface soil was very dry, although the recorded VWC at 10 cm was at 0.18 m^3·m^{-3}, which is not especially low. A similar result was observed on 5 July 2016, when the lowest soil moisture in the experimental period was recorded, at 0.14 m^3·m^{-3}, and a relatively low K_{fs} value was observed (Figure 8c). This reduced water infiltration may be attributable to water repellency of the soil [65,66], but it is also possible that an antecedent heavy storm or spray irrigation that fell on freshly harvested land during summer formed soil crusts which reduced the infiltration capacity of the surface soil [67].

The soil at the living filter tends to be cold and wet during winter [68], and this combined effect could explain the lower K_{fs} values in winter than in summer. Similar seasonal variations of K_{fs} were also observed in other regions and should be considered when planning wastewater treatment management and best management practices [12,14,15].

3.4. Long-Term Effects of Wastewater Irrigation on K_{fs}

In the irrigated cropland, at site K2, the observed minimum K_{fs} was 13.2 mm·h^{-1} and the maximum K_{fs} was 311.4 mm·h^{-1}, with a mean ± standard deviation (SD) of 97.9 ± 78.4 mm·h^{-1} and a CV of 80.1%. There were only six valid measurements at K3, with a minimum and maximum K_{fs} of 37.4 and 174.3 mm·h^{-1}, respectively, and a CV of 61.0%. Measurements at K3 were carried out in June 2017 and had a mean K_{fs} of 95.0 ± 57.9 mm·h^{-1}, without a significant difference from the results of K2 during the same time period. In the non-irrigated cropland, K1, the minimum and maximum K_{fs} values were 14.8 and 367.2 mm·h^{-1}, respectively, with a mean ± SD of 85.1 ± 87.4 mm·h^{-1} and a CV of 102.7%. The minimum of all results at all three sites was higher than the nominal application rate of the treated wastewater irrigation (4.25 mm·h^{-1}).

All viscosity-corrected K_{fs_STP} values from K1 and K2 were compared, and no significant difference (p = 0.357) was found (Figure 9). At site K1, the mean and SD of K_{fs_STP} was 103.2 ± 94.6,

while the results at site K2 were slightly higher at 123.8 ± 94.0 mm·h^{-1}. During winter, K_{fs_STP} values at K1 and K2 were 80.4 ± 52.9 and 107.0 ± 76.0 mm·h^{-1}, respectively, without a significant difference (p = 0.442). During summer, K_{fs_STP} at K1 and K2 were 127.1 ± 133.9 and 122.5 ± 101.7 mm·h^{-1}, respectively, also without a significant difference (p = 0.737).

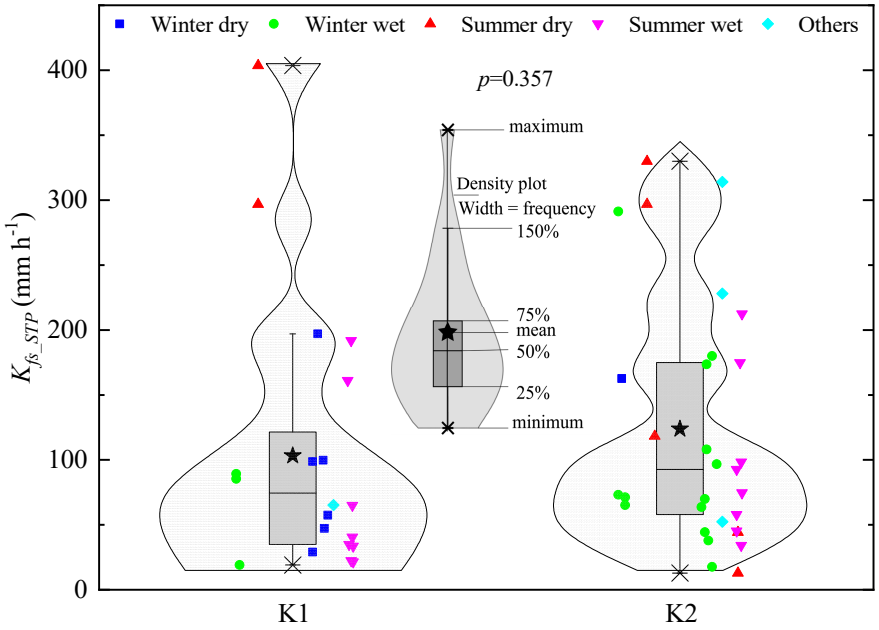

Figure 9. Viscosity-corrected field-saturated hydraulic conductivities (K_{fs_STP}) in the cropland without (K1) and with (K2) irrigation, including a total of 23 and 29 valid measurements, respectively, during the experimental period.

These results appear to be a bit different from previous findings in the same area. Sopper and Richenderfer [41] measured K_{fs} using DRI and found that there was a significant increase in infiltration on the irrigated corn-cropped land. Walker [69] also reported a higher hydraulic conductivity in irrigated areas than in control areas, as measured by the constant head method in a laboratory setting. Larson [70] measured hydraulic conductivity using a tension infiltrometer and showed that hydraulic conductivity was relatively higher in irrigated lands than in non-irrigated lands, especially at 3 and 6 cm of tension, suggesting that the increased hydraulic conductivity was mainly attributable to an increase in the abundance of soil pores with radii of 0.025 to 0.050 mm. Due to the difficulty of data acquisition, the high failure rate of the tests, and the inherent spatiotemporal variability of the measured parameter, this study was too statistically underpowered to definitively answer the question of the effects of long-term irrigation on K_{fs}. However, especially in light of other data collected at the same locations, it is likely that the increases observed here, although statistically insignificant, reflect real conditions in the soil. The insignificant results were due to limited replicated measurements at limited sites, combined with the considerable spatiotemporal variability of the measured parameter.

Several explanations were proposed to explain increased hydraulic conductivities in irrigated soils. Firstly, the nutrient-rich treated wastewater encourages plant growth and soil organic matter accumulation. A lush crop canopy offers protection from raindrop impacts, thereby decreasing surface soil compaction or crusting, while the activity of plant roots improves soil structure and increases macropores. Macropores may contribute nearly 85% of the variation of hydraulic conductivity or total infiltration [71,72], as suggested by the dramatic increase in the incidence of preferential flow at irrigated sites in the living filter [42]. In addition, the increase in nutrients from the effluent would tend to improve soil physicochemical properties. Treated wastewater irrigation was found to increase organic matter content and soil pH [29], while lower bulk densities and higher soil pH values and electrical conductivities were measured on irrigated croplands, as compared to

non-irrigated croplands [21,70]. These positive effects could result from higher organic matter inputs, increased soil fauna abundance, and plant root growth, as well as greater freeze–thaw cycling [73–75]. Many lines of evidence suggest that decades of spray irrigation caused physical adaptations in the irrigated soils at the living filter, which can accommodate much large volumes of water (beyond natural precipitation).

4. Summary and Conclusions

In situ measurements of two critical soil hydrologic parameters (*IR* and K_{fs}) at the living filter wastewater tertiary treatment system at the Pennsylvania State University were conducted during both winter and summer months using newly designed dualhead infiltrometers (DHIs) following both original (default) and optimized (modified) operation settings. The results were also compared with traditional double-ring infiltrometers (DRIs) measurements under various field conditions. The results of this study support the following conclusions:

(1) For the silt loam soil in our study site, the optimized DHI procedure, with one long cycle, achieved steadier pressure heads and infiltration rates and, therefore, yielded more credible K_{fs} values than the original two short-cycle default setting.
(2) The values of K_{fs} measured by the DHI were, for the most part, similar to those measured by DRI, but were higher under some conditions. This is likely due to the smaller infiltration area of the DRI we used, which possibly missed soil macropores.
(3) The values of viscosity-corrected K_{fs} from irrigated croplands were higher than those from non-irrigated croplands, but the difference was statistically insignificant (p = 0.357) due to high spatiotemporal variability and small sample sizes. Nevertheless, these results do suggest that the long-term application of wastewater irrigation at the site enhanced K_{fs}. Measured IR and K_{fs} values were all much higher than the actual spray irrigation rate under all conditions (4.25 $mm \cdot h^{-1}$). From this perspective, the current application of treated wastewater irrigation does not seem to be at high risk of causing overland flow, even under winter conditions with frozen ground.
(4) Values of IR and K_{fs} were lower during winter than during summer, as soil conditions tend to be cold and wet in the winter and warm and dry in the summer. Infiltration processes during winter should, therefore, receive extra attention when implementing wastewater irrigation systems, such as the one investigated here at Penn State's living filter.
(5) Values of IR and K_{fs} showed great spatiotemporal variability and some uncertainty, but they were clearly influenced by antecedent soil moisture and temperature conditions. Surprisingly, snow cover, cold air, and frozen soil did not show particularly significant impacts on winter IR and K_{fs} in this study. This is probably attributable to warmer soil temperatures associated with the thick layers of effluent that tend to build up on frozen soils after long periods of intense irrigation. This aids in preventing runoff in the living filter system by encouraging locally permeable frozen surfaces. The depth and temporal extent of frozen conditions, as well as the infiltration status and subsurface water fluxes under frozen conditions, require further investigation.

Author Contributions: H.L. designed the experiment and oversaw the project; I.H. collected data and co-designed the experiment; S.Z. analyzed the data and wrote the initial draft of the paper; L.G. helped with data organization and analysis. All authors contributed to the review, revision, and finalization of the manuscript.

Funding: This work was supported by the Penn State's Office of Physical Plant and US National Science Foundation Hydrologic Sciences Program Grant EAR-1416881 (PI: H. Lin), GDAS Project of Science and Technology Development (2019GDASYL-0401003 and 2019GDASYL-0102002), and Guangdong Provincial Science and Technology Project（2018B030324001）.

Acknowledgments: We thank Grace Billy, Chris Valdez, Zach Klueber, David Smilnak, and Heather Gall for their assistance with the field measurements.

Conflicts of Interest: The authors declare no conflicts of interest.

References

1. Rawls, W.J.; Nemes, A.; Pachepsky, Y. Effect of soil organic carbon on soil hydraulic properties. In *Developments in Soil Science*; Elsevier: Amsterdam, The Netherlands, 2004; pp. 95–114, doi:10.1016/S0166-2481(04)30006-1.
2. Tejedor, M.; Neris, J.; Jiménez, C. Soil properties controlling infiltration in volcanic soils (Tenerife, Spain). *Soil Sci. Soc. Am. J.* **2013**, *77*, 202, doi:10.2136/sssaj2012.0132.
3. Kumar, P. Studying Variability in Observed Soil Infiltration Rates as Influenced by Infiltrometers of Varied Configurations. Master's Thesis, Anand Agricultural University, Godhra, India, 2015.
4. Lin, H.S.; Mcinnes, K.J.; Wilding, L.P.; Hallmark, C.T. Macroporosity and initial moisture effects on infiltration rates in vertisols and vertic intergrades. *Soil Sci.* **1998**, *163*, 2–8, doi:10.1097/00010694-199801000-00002.
5. Briggs, L.J. *The Mechanics of Soil Moisture, USDA*; Division of Soils: Washington, DC, USA, 1897.
6. Hopmans, J.W.; Dane, J.H. Temperature dependence of soil hydraulic properties. *Soil Sci. Soc. Am. J.* **1986**, *50*, 4–9, doi:10.2136/sssaj1986.03615995005000010001x.
7. Ruggenthaler, R.; Mei, L.G.; Geitner, C.; Leitinger, G.; Endstrasser, N.; Sch Berl, F. Investigating the impact of initial soil moisture conditions on total infiltration by using an adapted double-ring infiltrometer. *Hydrol. Sci. J.* **2016**, *61*, 1217–1263, doi:10.1080/02626667.2015.1031758.
8. Turner, D.P.; Sumner, M.E. The influence of initial soil moisture content on field measured infiltration rates. *Water SA* **1978**, *4*, 18–24.
9. Wu, G.; Yang, Z.; Cui, Z.; Liu, Y.; Fang, N.; Shi, Z. Mixed artificial grasslands with more roots improved mine soil infiltration capacity. *J. Hydrol.* **2016**, *535*, 54–60, doi:10.1016/j.jhydrol.2016.01.059.
10. Thompson, S.E.; Harman, C.J.; Heine, P.; Katul, G.G. Vegetation-infiltration relationships across climatic and soil type gradients. Journal of Geophysical Research: *Biogeosciences* **2010**, *115*, doi:10.1029/2009JG001134.
11. Wu, G.; Liu, Y.; Yang, Z.; Cui, Z.; Deng, L.; Chang, X.; Shi, Z. Root channels to indicate the increase in soil matrix water infiltration capacity of arid reclaimed mine soils. *J. Hydrol.* **2017**, *546*, 133–139, doi:10.1016/j.jhydrol.2016.12.047.
12. Cerdà, A. Seasonal changes of the infiltration rates in a Mediterranean scrubland on limestone. *J. Hydrol.* **1997**, *198*, 209–225, doi:10.1016/S0022-1694(96)03295-7.
13. Hardie, M.A.; Doyle, R.B.; Cotching, W.E.; Mattern, K.; Lisson, S. Influence of antecedent soil moisture on hydraulic conductivity in a series of texture-contrast soils. *Hydrol. Process.* **2012**, *26*, 3079–3091, doi:10.1002/hyp.8325.
14. Cerdà, A.; Keesstra, S.; Burguet, M.; Pereira, P.; Lucasborja, M.E.; Martinezmurillo, J.F. Seasonal changes of the infiltration rates in urban parks of Valencia city, eastern Spain. Geophysical Research Abstracts. In Proceedings of the EGU General Assembly Conference, Vienna, Austria, 17–22 April 2016; p. 18110.
15. Emerson, C.H.; Traver, R.G. Multiyear and seasonal variation of infiltration from storm-water best management practices. *J. Irrig. Drain. Eng.* **2008**, *134*, 598–605, doi:10.1016/B978-0-12-385874-0.00008-X.
16. Fouli, Y.; Cade-Menun, B.J.; Cutforth, H.W. Freeze-thaw cycles and soil water content effects on infiltration rate of three Saskatchewan soils. *Can. J. Soil Sci.* **2013**, *93*, 485–496.
17. Iwata, Y.; Nemoto, M.; Hasegawa, S.; Yanai, Y.; Kuwao, K.; Hirota, T. Influence of rain, air temperature, and snow cover on subsequent spring-snowmelt infiltration into thin frozen soil layer in northern japan. *J. Hydrol.* **2011**, *401*, 165–176, doi:10.1016/j.jhydrol.2011.02.019.
18. Bdour, A.N.; Hamdi, M.R.; Tarawneh, Z. Perspectives on sustainable wastewater treatment technologies and reuse options in the urban areas of the Mediterranean region. *Desalination* **2009**, *237*, 162–174, doi:10.1016/j.desal.2007.12.030.
19. Coppola, A.; Santini, A.; Botti, P.; Vacca, S. Urban wastewater effects on water flow and solute transport in soils. *J. Environ. Sci. Health Part A* **2003**, *38*, 1469–1478, doi:10.1081/ESE-120021472.
20. Hati, K.; Biswas, A.; Bandyopadhyay, K.; Misra, A. Soil properties and crop yields on a vertisol in India with application of distillery effluent. *Soil Tillage Res.* **2007**, *92*, 60–68, doi:10.1016/j.still.2006.01.011.
21. Vogeler, I. Effect of long-term wastewater application on physical soil properties. *Water Air Soil Pollut.* **2009**, *196*, 385–392, doi:10.1007/s11270-008-9785-x.
22. Bhardwaj, A.K.; Goldstein, D.; Azenkot, A.; Levy, G.J. Irrigation with treated wastewater under two different irrigation methods: Effects on hydraulic conductivity of a clay soil. *Geoderma* **2007**, *140*, 199–206, doi:10.1016/j.geoderma.2007.04.003.

23. Sparling, G.P.; Williamson, J.C.; Magesan, G.N.; Schipper, L.A.; Lloyd-Jones, A.R. Hydraulic conductivity in soils irrigated with wastewaters of differing strengths: Field and laboratory studies. *Soil Res.* **1999**, *37*, 391–402, doi:10.1071/S98030.
24. Menneer, J.C.; Mclay, C.D.A.; Lee, R. Effects of sodium-contaminated wastewater on soil permeability of two New Zealand soils. *Soil Res.* **2001**, *39*, 877–891, doi:https://doi.org/10.1071/SR99082.
25. Wang, Z.; Chang, A.C.; Wu, L.; Crowley, D. Assessing the soil quality of long-term reclaimed wastewater-irrigated cropland. *Geoderma* **2003**, *114*, 261–278, doi:10.1016/S0016-7061(03)00044-2.
26. Coppola, A.; Santini, A.; Botti, P.; Vacca, S.; Comegna, V.; Severino, G. Methodological approach for evaluating the response of soil hydrological behavior to irrigation with treated municipal wastewater. *J. Hydrol.* **2004**, *292*, 114–134, doi:10.1016/j.jhydrol.2003.12.028.
27. Gharaibeh, M.A.; Eltaif, N.I.; Al-Abdullah, B. Impact of field application of treated wastewater on hydraulic properties of vertisols. *Water Air Soil Pollut.* **2007**, *184*, 347–353, doi:10.1007/s11270-007-9423-z.
28. Lado, M.; Benhur, M. Effects of irrigation with different effluents on saturated hydraulic conductivity of arid and semiarid soils. *Soil Sci. Soc. Am. J.* **2010**, *74*, 23–32, doi:10.2136/sssaj2009.0114.
29. Walker, C.; Lin, H.S. Soil property changes after four decades of wastewater irrigation: A landscape perspective. *Catena* **2008**, *73*, 63–74, doi:10.1016/j.catena.2007.09.002.
30. National Research Council (NRC). *Water Reuse: Expanding the Nation's Water Supply Through Reuse of Municipal Wastewater*; National Academies: Washington, DC, USA, 2012.
31. Fox, P.; Houston, S.; Westerhoff, P.; Drewes, J.E.; Nellor, M.; Yanko, W.; Baird, R.; Rincon, M.; Arnold, R.; Lansey, K.; et al. *Soil Aquifer Treatment for Sustainable Water Reuse*; American Water Works Association Research Foundation: Denver, CO, USA, 2001.
32. Parizek, R.R. Opportunities to enhance management of karstic aquifers. *Environ. Geol.* **2007**, *51*, 731–735, doi:10.1007/s00254-006-0392-0.
33. Penn State University Office of Physical Plant (PSUOPP). *Annual Report of the Penn State's Living Filter*; PSUOPP: University Park, PA, USA, 2011.
34. Angulo-Jaramillo, R.; Vandervaere, J.; Roulier, S.; Thony, J.; Gaudet, J.; Vauclin, M. Field measurement of soil surface hydraulic properties by disc and ring infiltrometers: A review and recent developments. *Soil Till. Res.* **2000**, *55*, 1–29, doi:10.1016/S0167-1987(00)00098-2.
35. Reynolds, W.D.; Elrick, D.E.; Youngs, E.G.; Amoozegar, A.; Booltink, H.; Bouma, J. Saturated and field-saturated water flow parameters. In *Methods of Soil Analysis. Part 4. Physical Methods*; Dane, J.H., Topp, G.C., Eds.; SSSA: Madison, WI, USA, 2002; pp. 797–801.
36. Decagon Devices. Dualhead Infiltrometer Operator's Manual; Decagon Devices: Pullman, WA, USA, 2015..
37. Nimmo, J.R.; Schmidt, K.M.; Perkins, K.S.; Stock, J.D. Rapid measurement of field-saturated hydraulic conductivity for areal characterization. *Vadose Zone J.* **2009**, *8*, 142, doi:10.2136/vzj2007.0159.
38. Ravi, S.; Wang, L.; Kaseke, K.F.; Buynevich, I.V.; Marais, E. Ecohydrological interactions within "fairy circles" in the Namib Desert: Revisiting the self-organization hypothesis. *J. Geophys. Res. Biogeosci.* **2017**, *122*, 405–414, doi:10.1002/2016JG003604.
39. Demirtas, I. Effects of Post-Fire Salvage Logging on Compaction, Infiltration, Water Repellency, and Sediment Yield and the Effectiveness of Subsoiling on Skid Trails. Master's Thesis, Michigan Technological University, Houghton, MI, USA, 2017.
40. Gonzales, H.B.; Ravi, S.; Li, J.; Sankey, J.B. Ecohydrological implications of aeolian sediment trapping by sparse vegetation in drylands. *Ecohydrology* **2018**, *11*, e1986, doi:10.1002/eco.1986.
41. Sopper, W.E.; Richenderfer, J.L. *Effects of Spray Irrigation of Municipal Wastewater on the Physical Properties of the Soil, Institute for Research on Land and Water Resources*; The Pennsylvania State University: University Park, PA, USA, 1978.
42. Hopkins, I.; Gall, H.; Lin, H. Natural and anthropogenic controls on the frequency of preferential flow occurrence in a wastewater spray irrigation field. *Agric. Water Manag.* **2016**, *178*, 248–257, doi:10.1016/j.agwat.2016.09.011.
43. Ferguson, B.K. Environmental planning for wastewater land application: Lessons from Penn State's living filter. *Landsc. Plan.* **1983**, *10*, 205–218, doi:10.1016/0304-3924(83)90048-5.
44. Parizek, R.; Nemitz, J.; Moret, G. *Flow and Water Quality Monitoring Data for Toftrees Resort and Country Club, Office of the Physical Plant.*; The Pennsylvania State University: State College, PA, USA, 2006.
45. USDA-NRCS. Available online: https://wcc.sc.egov.usda.gov/nwcc/site?sitenum=2036 (accessed on 6 June 2018).

46. Shi, S. *General Theory of Statistics*; Tsinghua University Press: Beijing, China, 2007. (In Chinese)
47. Reynolds, W.D.; Elrick, D.E. Ponded infiltration from a single ring: I. Analysis of steady flow. *Soil Sci. Soc. Am. J.* **1990**, *54*, 1233–1241, doi:10.2136/sssaj1990.03615995005400050006x.
48. Hillel, D. *Environmental Soil Physics: Fundamentals, Applications, and Environmental Considerations*; Academic Press: San Diego, CA, USA, 1998.
49. Clancy, K.; Alba, V.M. Temperature and time of day influence on double-ring infiltrometer steady-state infiltration rates. *Soil Sci. Soc. Am. J.* **2011**, *75*, 241–245, doi:10.2136/sssaj2009.0355N.
50. Philip, J.R. The theory of infiltration: 1. The infiltration equation and its solution. *Soil Sci.* **1957**, *83*, 345–358.
51. Brutsaert, W. The concise formulation of diffusive sorption of water in a dry soil. *Water Resour. Res.* **1976**, *12*, 1118–1124, doi:10.1029/WR012i006p01118.
52. Youngs, E.G. An estimation of sorptivity for infiltration studies from moisture moment considerations. *Soil Sci.* **1968**, *106*, 157–163.
53. Lai, J.; Ren, L. Assessing the size dependency of measured hydraulic conductivity using double-ring infiltrometers and numerical simulation. *Soil Sci. Soc. Am. J.* **2007**, *71*, 1667, doi:10.2136/sssaj2006.0227.
54. Schulze Makuch, D.; Carlson, D.A.; Cherkauer, D.S.; Malik, P. Scale dependency of hydraulic conductivity in heterogeneous media. *Groundwater* **1999**, *37*, 904–919, doi:10.1111/j.1745-6584.1999.tb01190.x.
55. Filipovic, V.; Weninger, T.; Filipovic, L.; Schwen, A.; Bristow, K.L.; Zechmeister-Boltenstern, S.; Leitner, S. Inverse estimation of soil hydraulic properties and water repellency following artificially induced drought stress. *J. Hydrol. Hydromech.* **2018**, *66*, 170–180, doi:10.2478/johh-2018-0002.
56. Farrick, K.K.; Akweli, Z.; Wuddivira, M.N. Influence of manure, compost additions and temperature on the water repellency of tropical soils. *Soil Res.* **2018**, *56*, 685–695, doi:10.1071/SR17303.
57. Gamie, R.; De Smedt, F. Experimental and statistical study of saturated hydraulic conductivity and relations with other soil properties of a desert soil. *Eur. J. Soil Sci.* **2018**, *69*, 256–264, doi:10.1111/ejss.12519.
58. Graham, C.; Lin, H.S. *Real-Time Soil Temperature and Moisture Monitoring at the Penn State Living Filter—Astronomy Site*; Penn State University Office of Physical Plant: University Park, PA, USA, 2010.
59. Hopkins, I.; Lin, H.S. *Continued Real-Time Soil Temperature and Moisture Monitoring at the Penn State Living Filter—Astronomy Site*; Penn State University Office of Physical Plant: University Park, PA, USA, 2012.
60. Duke, H.R. Water temperature fluctuations and effect on irrigation infiltration. *Trans. ASAE* **1992**, *35*, 193–199, doi:10.13031/2013.28587.
61. Levy, G.J.; Smith, H.J.C.; Agassi, M. Water temperature effect on hydraulic conductivity and infiltration rate of soils. *S. Afr. J. Plant Soil* **1989**, *6*, 240–244, doi:10.1080/02571862.1989.10634520.
62. Constantz, J.; Herkelrath, W.N.; Murphy, F. Air encapsulation during infiltration. *Soil Sci. Soc. Am. J.* **1988**, *52*, 10–16, doi:10.2136/sssaj1988.03615995005200010002x.
63. Bond, W.J.; Collisgeorge, N. Ponded infiltration into simple soil systems 1. The saturation and transition zones in the moisture-content profiles. *Soil Sci.* **1981**, *131*, 202–209, doi:10.1097/00010694-198104000-00002.
64. Philip, J.R. The theory of infiltration: 5. The influence of the initial moisture content. *Soil Sci.* **1957**, *84*, 329–340.
65. Doerr, S.H.; Thomas, A.D. The role of soil moisture in controlling water repellency: New evidence from forest soils in Portugal. *J. Hydrol.* **2000**, *231–232*, 134–147, doi:10.1016/S0022-1694(00)00190-6.
66. Wang, Z.; Wu, L.; Wu, Q.J.; Ritsema, C.J.; Dekker, L.W.; Feyen, J. Effects of soil water repellency on infiltration rate and flow instability. *J. Hydrol.* **2000**, *231–232*, 265–276, doi:10.1016/S0022-1694(00)00200-6.
67. Vandervaere, J.P.; Peugeot, C.; Vauclin, M.; Angulo Jaramillo, R.; Lebel, T. Estimating hydraulic conductivity of crusted soils using disc infiltrometers and minitensiometers. *J. Hydrol.* **1997**, *188*, 203–223, doi:10.1016/S0022-1694(96)03160-5.
68. Hopkins, I. Soil Hydrology at the Living Filter: Analysis of Preferential Flow and Moisture-Temperature Dynamics under Wastewater Irrigation. Master's Thesis, The Pennsylvania State University, State College, PA, USA, 2016.
69. Walker, C.W. Enhanced Techniques for Determining Changes to Soils Receiving Wastewater Irrigation for over Forty Years. Doctor's Thesis, The Pennsylvania State University, State College, PA, USA, 2006.
70. Larson, Z.M. Long-Term Treated Wastewater Irrigation Effects on Hydraulic Conductivity and Soil Quality at Penn State's Living Filter; The Pennsylvania State University, State College, PA, USA, 2010.
71. Liu, M.; Wu, D.; Wu, S.; Liao, L. Characteristic of soil macropores under various types of forest coverage and their influence on saturated hydraulic conductivity in the Three Gorges Reservoir Area. *Acta Ecol. Sin.* **2016**, *36*, 3189–3196, doi:10.5846 /stxb201504280880.

72. Cameira, M.R.; Fernando, R.M.; Pereira, L.S. Soil macropore dynamics affected by tillage and irrigation for a silty loam alluvial soil in southern Portugal. *Soil Tillage Res.* **2003**, *70*, 131–140, doi:10.1016/S0167-1987(02)00154-X.
73. Bronick, C.J.; Lal, R. Soil structure and management: A review. *Geoderma* **2005**, *124*, 3–22, doi:10.1016/j.geoderma.2004.03.005.
74. Oades, J.M. Soil organic matter and structural stability: Mechanisms and implications for management. *Plant. Soil* **1984**, *76*, 319–337, doi:10.1007/BF02205590.
75. Frey, S.D.; Elliott, E.T.; Paustian, K. Bacterial and fungal abundance and biomass in conventional and no-tillage agroecosystems along two climatic gradients. *Soil Biol. Biochem.* **1999**, *31*, 573–585, doi:10.1016/S0038-0717(98)00161-8.